Sticky complexes: carboxylic acid-functionalized N-phenylpyridin-2-ylmethanimine ligands as anchoring domains for copper and ruthenium dye-sensitized solar cells†

Biljana Bozic-Weber, Edwin C. Constable,* Catherine E. Housecroft,* Markus Neuburger and Jason R. Price

Four members of a series of N-phenylpyridin-2-ylmethanimine ligands (L) decorated with carboxylic acid functionalities have been prepared. The ligand design allows a copper(I) complex $[CuL_2]^+$ to bind to a TiO_2 surface through the simultaneous use of two carboxylate anchoring domains. Complexes of the type $[CuL_2][PF_6]$, $[CuL(NCMe)_2][PF_6]$ and $[Ru(bpy)_2L][PF_6]_2$ have been synthesized and characterized by ^1H and ^{13}C NMR and electronic absorption spectroscopies, mass spectrometry and, for four of the complexes, single crystal X-ray diffraction. Dye-sensitized solar cells (DSCs) have been fabricated using the new complexes and the performances of the dyes assessed. The copper(I) complexes show good surface coverage and tuning of the electrolyte and the electronic properties of the ligands is now required to enhance the efficiencies of the DSCs.

Introduction

Carboxylate-functionalized complexes are ubiquitous among the dyes that bind to TiO_2 nanoparticles in dye-sensitized solar cells (DSCs).[1-4] Since the initial reports of a $[Ru(bpy)_3]^{2+}$-based (bpy = 2,2′-bipyridine) photosensitizer,[5,6] the dyes reported in the literature have predominantly been ruthenium(II) complexes. In terms of cost and natural abundance, however, ruthenium is not ideal. As a consequence, we have recently become interested in the development of copper(I)-based DSCs,[7] literature reports of which are scarce.[8-11] We have discovered that carboxylate-derivatized copper(I) bis(2,2′-bipyridine) complexes can successfully be employed to fabricate efficient DSCs,[7] and we are currently synthesizing and screening a wide range of copper(I) complexes functionalized with substituents designed to anchor the complex to a TiO_2 surface.[12,13] For the copper(I) complexes to be stable with respect to aerial oxidation, it is necessary to incorporate substituents at the 6- and 6′-positions[14] which sterically protect the metal centre and modulate the redox properties. Imines are also known to stabilize copper(I) and a wide variety of copper(I) complexes containing imine-based ligands is documented in the literature. Iminopyridine ligands provide a bpy-like metal-binding domain and have been widely exploited in the formation of mono- and multinuclear copper complexes,[15] in catalysis[16] and for dynamic libraries.[17] The ease of synthesis of iminopyridine Schiff base ligands makes them an attractive alternative to the electronically similar functionalized bpy ligands. In this report, we describe the formation of ruthenium(II) and copper(I) complexes containing ligands 1–4 (Scheme 1) and assess the performance of the $[CuL_2]^+$ (L = 3 or 4) complexes in comparison to $[Ru(bpy)_2L]^{2+}$ (L = 1 or 2) dyes in DSCs. The ligands have been designed so that, in the

Department of Chemistry, University of Basel, Spitalstrasse 51, CH 4056, Basel, Switzerland. E-mail: catherine.housecroft@unibas.ch, edwin. constable@unibas.ch; Fax: +41 61 267 1018; Tel: +41 61 267 1008/1001
† CCDC reference numbers 756938–756941. For crystallographic data in CIF or other electronic format see DOI: 10.1039/b925623g
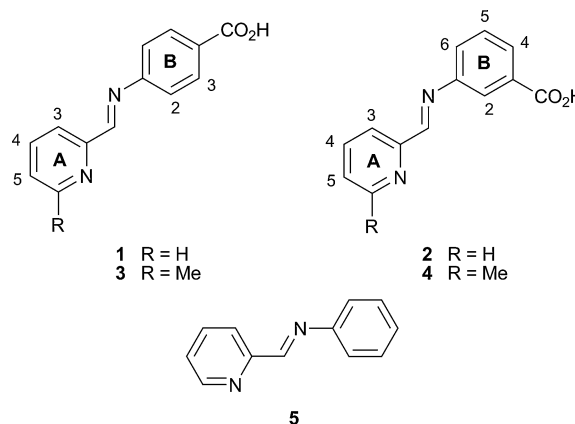
Scheme 1 Ligand structures and atom labelling for NMR spectroscopic assignments.

$[CuL_2]^+$ complexes which are expected to be near tetrahedral at the metal centre, both carboxylate anchoring groups may interact with the TiO_2 surface (Scheme 2).
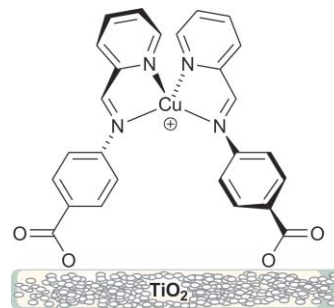
Scheme 2 Proposed mode of binding of $[CuL_2]^+$ (L = 1 or 3) to a TiO_2 surface. A similar mode is proposed for $[CuL_2]^+$ (L = 2 or 4).

Experimental

General

^{1}H and ^{13}C NMR spectra were recorded at room temperature on a Bruker Avance DRX 500 MHz spectrometer; chemical shifts are relative to residual solvent peaks (TMS δ 0 ppm). Electrospray ionisation (ESI) mass spectra were recorded on a Bruker esquire 3000^{plus} mass spectrometer. Electronic absorption and emission spectra were recorded on a Varian-Cary 5000 spectrophotometer and Shimadzu RF-5301 PC spectrofluorometer, respectively. Microwave reactions were carried out in a Biotage Initiator 8 reactor. Solvents were distilled before use and their water content was monitored by Karl Fischer titration.

Preparation and evaluation of solar cells

Nanocrystalline TiO_2 electrodes were prepared by doctor blading a colloidal TiO_2 paste (Solaronix Nanooxide-T, colloidal anatase) onto a conducting glass slide (F-doped SnO_2, FTO, Hartford glass company, Tec 8, 8 Ω cm^{-2}) to give a 6 μm thick film. After annealing at 450 °C for 30 min, the slides were dipped into a solution (3 mmol dm^{-3}) of the dye in MeCN for the ruthenium(II) complexes and DMF for the copper(I) complexes for several hours. The cells were made using LiI (0.5 mol dm^{-3}), I_2 (0.05 mol dm^{-3}), 1-methylbenzimidazole (0.5 mol dm^{-3}) and 1-butyl-3-methylimidazolinium iodide (0.6 mol dm^{-3}) in 3-methoxypropionitrile as the electrolyte. The electrolyte was chosen to give the best comparison to the state-of-the-art optimized systems based on N719 (standard dye from Solaronix). Cathodes (the same size as the anodes) were made from FTO glass pieces platinized by treatment with H_2PtCl_6 (5 mmol dm^{-3}) in propan-2-ol, followed by heating to 280 °C for 15 min. The anode and cathode were assembled using Surlyn (Dupont) plastic by heating while pressing the two together. Measurements were made by irradiating from behind using a light source SolarSim 150 (100 mW cm^{-2} = 1 sun).

The precursors cis-[Ru(bpy)$_2$Cl$_2$][18] and [Cu(NCMe)$_4$][PF$_6$][19] were prepared as previously described.

Ligand 1

Ligand **1** was prepared according to the literature procedure.[20] NMR spectroscopic data have not previously been reported. ^{1}H NMR (500 MHz, CD$_3$OD) δ (ppm) 8.70 (d, J 4.4 Hz, 1H, H^{A6}), 8.59 (s, 1H, H$^{HC=N}$), 8.23 (d, J 7.9 Hz, 1H, H^{A3}), 8.10 (d, J 8.3 Hz, 2H, H^{B3}), 7.99 (t, J 7.6 Hz, 1H, H^{A4}), 7.55 (m, 1H, H^{A5}), 7.34 (d, J 8.4 Hz, 2H, H^{B2}). ^{1}H NMR (500 MHz, DMSO-d_6) δ (ppm) 12.5 (br, CO$_2$H), 8.75 (d, J 4.7 Hz, 1H, H^{A6}), 8.59 (s, 1H, H$^{HC=N}$), 8.17 (d, J 7.9 Hz, 1H, H^{A3}), 8.00 (d, J 8.4 Hz, 2H, H^{B3}), 7.99 (td, J 7.7, 1.2 Hz, 1H, H^{A4}), 7.58 (m, 1H, H^{A5}), 7.39 (d, J 8.4 Hz, 2H, H^{B2}); ESI-MS m/z 281.2 [M + Na + MeOH]$^+$ (base peak, calc. 281.1), 249.2 [M + Na]$^+$ (calc. 249.1), 227.2 [M + H]$^+$ (calc. 227.1); see text.

Ligand 2

Ligand **2** was synthesized as previously reported.[21] ^{1}H NMR spectroscopic data were not assigned[21] and are given here. ^{1}H NMR (500 MHz, CD$_3$OD) δ (ppm) 8.68 (d, J 4.6 Hz, 1H, H^{A6}),

8.62 (s, 1H, H$^{HC=N}$), 8.22 (d, J 7.9 Hz, 1H, H^{A3}), 7.96 (m, 2H, H^{A4+B4}), 7.92 (s, 1H, H^{B2}), 7.54 (m, 3H, H$^{A5+B5+B6}$); ESI-MS m/z 281.2 [M + Na + MeOH]$^+$ (calc. 281.1), 249.2 [M + Na]$^+$ (base peak,calc. 249.1), 227.2 [M + H]$^+$ (calc. 227.1); see text.

Ligand 3

A suspension of 6-methylpyridine-2-carbaldehyde (1.08 g, 8.92 mmol) and 4-aminobenzoic acid (1.22 g, 8.90 mmol) in EtOH (25 cm^3) was heated at reflux for 1 h. The reaction mixture was evaporated to dryness under reduced pressure and the crude product was recrystallized from ethyl acetate. Compound **3** was isolated as a pale yellow powder (1.72 g, 80.5%). ^{1}H NMR (500 MHz, CD$_3$OD) δ (ppm) 8.56 (s, 1H, H$^{HC=N}$), 8.09 (d, J 8.1 Hz, 2H, H^{B3}), 8.03 (d, J 7.7 Hz, 1H, H^{A3}), 7.86 (t, J 7.8 Hz, 1H, H^{A4}), 7.42 (d, J 7.7 Hz, 1H, H^{A5}), 7.33 (d, J 8.1 Hz, 2H, H^{B2}), 2.62 (s, 3H, H^{Me}); see text. ESI-MS m/z 241.2 [M + H]$^+$ (base peak, calc. 241.1), 263.1 [M + Na]$^+$ (calc. 263.1), 295.1 [M + MeOH + Na]$^+$ (calc. 295.1). Found C 69.36, H 5.39, N 11.38; $C_{14}H_{12}N_2O_2$ requires C 69.99, H 5.03, N 11.66%.

Ligand 4

A suspension of 6-methylpyridine-2-carbaldehyde (0.99 g, 8.17 mmol) and 3-aminobenzoic acid (1.12 g, 8.17 mmol) in EtOH (25 cm^3) was heated at reflux for 1 h. The reaction mixture was evaporated to dryness under reduced pressure and the crude product recrystallized from EtOH. Compound **4** was isolated as an off-white powder (1.41 g, 71.8%). ^{1}H NMR (500 MHz, CD$_3$OD) δ (ppm) 8.57 (s, 1H, H$^{HC=N}$), 8.01 (d, J 7.7 Hz, 1H, H^{A3}), 7.93 (d, J 7.2 Hz, 1H, H^{B4}), 7.90 (s, 1H, H^{B2}), 7.84 (t, J 7.7 Hz, 1H, H^{A4}), 7.51 (m, 2H, H^{B6+B5}), 7.39 (m, 1H, H^{A5}), 2.60 (s, 3H, H^{Me}); see text. ESI-MS m/z 241.3 [M + H]$^+$ (calc. 241.1), 263.2 [M + Na]$^+$ (base peak, calc. 263.1), 295.1 [M + MeOH + Na]$^+$ (calc. 295.1). Found C 69.65, H 5.21, N 11.56; $C_{14}H_{12}N_2O_2$ requires C 69.99, H 5.03, N 11.66%.

[Ru(bpy)$_2$(1)][PF$_6$]$_2$

Ligand **1** (50.0 mg, 0.221 mmol) and cis-[Ru(bpy)$_2$Cl$_2$] (108.5 mg, 0.224 mmol) were suspended in EtOH (4 cm^3). The reaction mixture was sealed in a microwave tube and heated at 140 °C for 10 min. The dark red-brown mixture was added to aqueous NH$_4$PF$_6$ (365 mg, 2.24 mol, 50 cm^3) and extracted with CH$_2$Cl$_2$–MeCN. The organic phase was washed with H$_2$O (3 × 25 cm^3) dried over MgSO$_4$·2H$_2$O and evaporated to dryness under reduced pressure. The crude product was dissolved in a minimum of MeCN ($ca.$ 2 cm^3) and Et$_2$O was allowed to diffuse into the solution overnight. The dark red/orange microcrystalline product was separated by filtration, washed with Et$_2$O and then dried under vacuum over P$_2$O$_5$. [Ru(bpy)$_2$(**1**)][PF$_6$]$_2$ was isolated as a red solid (107 mg, 52.1%). ^{1}H NMR (500 MHz, CD$_3$CN) δ (ppm) 9.08 (s, 1H, H$^{HC=N}$), 8.55 (m, 3H, H$^{E3+E6+F3}$), 8.36 (d, J 7.8 Hz, 1H, H^{A3}), 8.21 (d, J 8.1 Hz, 1H, H^{C3}), 8.16 (t, J 7.3 Hz, 1H, H^{E4}), 8.09 (m, 3H, H$^{A4+C4+F4}$), 7.99 (d, J 8.2 Hz, 1H, H^{D3}), 7.83 (d, J 5.5 Hz, 1H, H^{A6}), 7.75 (m, 2H, H^{D4+F6}), 7.70 (d, J 5.5 Hz, 1H, H^{C6}), 7.62 (d, J 8.4 Hz, 2H, H^{B3}), 7.60 (t, J 7.0 Hz, 1H, H^{E5}), 7.54 (d, J 6.5 Hz, 1H, H^{D6}), 7.53 (t, J 6.5 Hz, 1H, H^{C5}), 7.50 (t, J 6.7 Hz, 1H, H^{A5}), 7.39 (t, J 6.5 Hz, 1H, H^{F5}), 7.22 (t, J 6.5 Hz, 1H, H^{D5}), 6.64 (d, J 8.4 Hz, 2H, H^{B2}), (OH not observed). ^{13}C NMR (126 MHz,

CD$_3$CN) δ (ppm) 170.6 (C$^{C=N}$), 166.4, 157.7, 157.6, 157.2, 154.0 (C^{F6}), 153.3 (C^{E6}), 153.2 (C^{A6}), 152.9, 152.8 (C^{C6}), 152.7 (C^{D6}), 139.4 (C^{C4}), 139.25 (C^{A4}), 139.2 (C^{E4}), 138.8 (C^{F4}), 138.6 (C^{D4}), 131.9 (C^{A3}), 131.5 (C^{B3}), 130.8 (C^{B4}), 130.2 (C^{A5}), 129.0 (C^{C5}), 128.9 (C^{E5}), 128.6 (C^{F5}), 128.3 (C^{D5}), 125.6 (C$^{E3/F3}$), 125.4 (C$^{E3/F3}$), 124.7 (C^{C3}), 124.4 (C^{D3}), 122.5 (C^{B2}) (2 signals not observed). UV/VIS (MeCN) λ_{max}/nm 244 (ε/dm^3 mol^{-1} cm^{-1} 30 900), 287 (66 000), 431 (9800), 486 (9500). ESI-MS: m/z 785.1 [M − PF$_6$]$^+$ (calc. 785.1), 320.0 [M − 2PF$_6$]$^{2+}$ (calc. 320.1). Found C 42.24, H 2.88, N 8.95; C$_{33}$H$_{26}$F$_{12}$N$_6$O$_2$P$_2$Ru·0.5H$_2$O requires C 42.23, H 2.90, N 8.95%.

[Ru(bpy)$_2$(2)][PF$_6$]$_2$

The method was as for [Ru(bpy)$_2$(1)][PF$_6$]$_2$, starting with ligand **2** (48.6 mg, 0.215 mmol) and *cis*-[Ru(bpy)$_2$Cl$_2$] (106 mg, 0.218 mmol). [Ru(bpy)$_2$(2)][PF$_6$]$_2$ was isolated as a red solid (43.9 mg, 22.0%). ^{1}H NMR (500 MHz, CD$_3$CN) δ (ppm) 9.09 (s, 1H, H$^{HC=N}$), 8.55 (m, 3H, H$^{E3+E6+F3}$), 8.34 (d, J 7.9 Hz, 1H, H^{A3}), 8.22 (d, J 8.1 Hz, 1H, H^{C3}), 8.15 (t, J 7.8 Hz, H^{E4}), 8.10 (m, 3H, H$^{A4+C4+F4}$), 8.00 (d, J 8.2 Hz, 1H, H^{D3}), 7.83 (d, J 5.5 Hz, 1H, H^{A6}), 7.75 (m, 3H, H$^{B4+D4+F6}$), 7.72 (d, J 5.8 Hz, 1H, H^{C6}), 7.58 (m, 2H, H^{D6+E5}), 7.53 (t, J 6.5 Hz, 1H, H^{C5}), 7.50 (t, J 6.6 Hz, 1H, H^{A5}), 7.39 (t, J 6.6 Hz, 1H, H^{F5}), 7.17 (m, 2H, H^{D5+B5}), 6.99 (s, 1H, H^{B2}), 6.92 (d, J 7.9 Hz, 1H, H^{B6}), 2.2 (OH not observed). ^{13}C NMR (126 MHz, CD$_3$CN) δ (ppm) 170.5 (C$^{C=N}$), 157.9, 157.8, 157.7, 157.6, 153.9 (C^{E6}), 153.4 (C^{A6}), 153.2 (C^{C6}), 152.9 (C^{F6}), 152.5 (C^{D6}), 139.2/139.1 (C$^{A4+C4+E4+F4}$), 138.8 (C^{D4}), 131.9 (C^{A3}), 130.6 (C^{B4+B5}), 130.0 (C^{A5}), 129.0 (C^{C5}), 128.9 (C^{E5}), 128.6 (C^{F5}), 128.4 (C^{D5}), 126.7 (C^{B6}), 125.6 (C^{E3+F3}), 124.8 (C^{C3}), 124.6 (C^{D3}), 123.2 (C^{B2}) (3 signals not observed). UV/VIS (MeCN) λ_{max}/nm 240 (ε/dm^3 mol^{-1} cm^{-1} 28 200), 287 (62 000), 435 (10 400), 482 (10 300). ESI-MS: m/z 785.2 [M − PF$_6$]$^+$ (calc. 785.1), 320.3 [M − 2PF$_6$]$^{2+}$ (calc. 320.1). Found C 41.15, H 3.14, N 8.62; C$_{33}$H$_{26}$F$_{12}$N$_6$O$_2$P$_2$Ru·2H$_2$O requires C 41.05, H 3.13, N 8.70%.

[Cu(3)$_2$][PF$_6$]

A MeCN (25 cm^3) solution of ligand **3** (122.9 mg, 0.512 mmol) was heated to reflux and degassed with N$_2$ for 15 min. [Cu(NCMe)$_4$][PF$_6$] (95.4 mg, 0.256 mmol) was then added, and the solution immediately turned dark red. The reaction mixture was heated at reflux under N$_2$ for 1 h and was then allowed to cool to room temperature. The mixture was filtered, concentrated under reduced pressure to one-third of the volume and placed in a sealed jar which contained Et$_2$O under N$_2$. After 2 d, the solid which had formed was separated by filtration and washed with Et$_2$O and dried over P$_2$O$_5$. [Cu(3)$_2$][PF$_6$] was isolated as a dark red-brown microcrystalline solid (149 mg, 84.4%). ^{1}H NMR (500 MHz, CD$_3$CN) δ (ppm) 9.08 (s, 1H, H$^{HC=N}$), 8.08 (t, 7.6 Hz, 1H, H^{A4}), 8.00 (br d, J ≈ 6 Hz, 2H, H^{B3}), 7.93 (d, J 7.5 Hz, 1H, H^{A5}), 7.67 (d, J 7.7 Hz, 1H, H^{A3}), 7.54 (br d, J ≈ 6 Hz, 2H, H^{B2}), 2.43 (s, 3H, H^{Me}). ^{13}C NMR (126 MHz, CD$_3$CN) 165.1 (C$^{C=N}$), 162.1 (C^{A2}), 159.7 (C^{A6}), 152.0 (C$^{B1/B4}$), 151.1 (C$^{B1/B4}$), 139.8 (C^{A4}), 132.7 (C^{B3}), 130.0 (C^{A3}), 127.3 (C^{A5}), 123.6 (C^{B2}), 25.5 (C^{Me}) (CO$_2$H carbon not observed). UV/VIS (MeCN) λ_{max}/nm 260 (ε/dm^3 mol^{-1} cm^{-1} 27 000), 310 (30 000), 511 (1000). ESI-MS: m/z 543.0 [M − PF$_6$]$^+$ (calc. 543.1). Found C 47.73, H 3.61, N 8.14; C$_{28}$H$_{24}$CuF$_6$N$_4$O$_4$P·H$_2$O requires C 47.57, H 3.71, N 7.92%.

[Cu(4)$_2$][PF$_6$]

A MeCN (25 cm^3) solution of ligand **4** (117.3 mg, 0.488 mmol) was heated to reflux and degassed with N$_2$ for 15 min, after which time [Cu(NCMe)$_4$][PF$_6$] (91.0 mg, 0.244 mmol) was added. The solution immediately turned dark red and was heated at reflux under N$_2$ for 1 h. After cooling to room temperature, the reaction mixture was filtered and the solvent removed under reduced pressure. The crude product was recrystallized from ethyl acetate–hexane and [Cu(4)$_2$][PF$_6$] was isolated as a dark red-brown microcrystalline solid (57.0 mg, 33.9%). ^{1}H NMR (500 MHz, CD$_3$CN) δ (ppm) 9.15 (s, 1H, H$^{HC=N}$), 8.08 (t, 7.6 Hz, 1H, H^{A4}), 8.07 (s, 1H, H^{B2}), 7.93 (overlapping d, J 7.7 Hz, 2H, H^{A3+B6}), 7.66 (m, 2H, H^{A5+B4}), 7.48 (t, J 7.8 Hz, 1H, H^{B5}), 2.41 (s, 3H, H^{Me}). ^{13}C NMR (126 MHz, CD$_3$CN) 171.0 (C$^{C=N}$), 161.3 (C^{A2}), 159.6 (C^{A6}), 151.4 (C$^{B1/B3}$), 148.4 (C$^{B1/B3}$), 139.7 (C^{A4}), 131.1 (C^{B5}), 130.7 (C^{A3}), 129.8 (C^{A5}), 128.1 (C$^{B4/B6}$), 127.1 (C$^{B4/B6}$), 123.9 (C^{B2}), 25.5 (C^{Me}) (CO$_2$H carbon not observed). UV/VIS (MeCN) λ_{max}/nm 282 nm (ε/dm^3 mol^{-1} cm^{-1} 15 400), 313 (16 800), 499 (1700). ESI-MS: m/z 543.0 [M − PF$_6$]$^+$ (calc. 543.1). Found C 48.74, H 3.59, N 8.07; C$_{28}$H$_{24}$CuF$_6$N$_4$O$_4$P requires C 48.81, H 3.51, N 8.13%.

[Cu(4)(NCMe)$_2$][PF$_6$]

The method was as for [Cu(4)$_2$][PF$_6$], but starting with ligand **4** (118.1 mg, 0.492 mmol) and [Cu(NCMe)$_4$][PF$_6$] (180.9 mg, 0.485 mmol). [Cu(4)(NCMe)$_2$][PF$_6$] was isolated as a red-brown crystalline solid (163 mg, 63.3%). ^{1}H NMR (500 MHz, CD$_3$CN) δ (ppm) 9.02 (s, 1H, H$^{HC=N}$), 8.18 (br s, 1H, H^{B2}), 8.07 (t, 7.7 Hz, 1H, H^{A4}), 8.00 (br d, J ≈ 7 Hz, 1H, H^{B6}), 7.87 (d, J 7.7 Hz, 1H, H^{A3}), 7.78 (br d, 1H, H^{B4}), 7.68 (d, J 7.8 Hz, 1H, H^{A5}), 7.58 (br t, 1H, H^{B5}), 2.60 (br s, 3H, H^{Me}), 1.96 (s, 6H, H^{MeCN}). ^{13}C NMR (126 MHz, CD$_3$CN), 161.1 (C^{A2}), 159.7 (C^{A6}), 151.1 (C$^{B1/B3}$), 150.9 (C$^{B1/B3}$), 139.9 (C^{A4}), 131.1 (br, C^{B5+B6}), 129.8 (C^{A5}), 128.1 (C^{B4}), 127.1 (C^{A3}), 124.0 (br, C^{B2}), 25.5 (C^{Me}) (C=N and CO$_2$H carbons not observed; MeCN carbons obscured by solvent peaks). UV/VIS (MeCN) λ_{max}/nm 312 (ε/dm^3 mol^{-1} cm^{-1} 18 000), 502 (2500). ESI-MS m/z 344.0 [M − PF$_6$ − MeCN]$^+$ (calc. 344.1). Found C 40.49, H 3.43, N 10.52; C$_{18}$H$_{18}$CuF$_6$N$_4$O$_2$P requires C 40.72, H 3.42, N 10.55%.

Crystal structure determinations†

Data were collected on a Bruker-Nonius Kappa CCD diffractometer; data reduction, solution and refinement used the programs COLLECT,[22] SIR92,[23] DENZO/SCALEPACK[24] and CRYSTALS.[25] Hydrogen atoms attached to O atoms were located from the difference maps. ORTEP figures were drawn using Ortep-3 for Windows.[26] Structures have been analysed using Mercury v. 2.2.[27]

[Cu(3)$_2$][PF$_6$]·2DMF

C$_{34}$H$_{38}$CuF$_6$N$_6$O$_6$P, M = 835.22, red plate, monoclinic, space group $C2/c$, a = 18.2661(13), b = 16.4632(13), c = 12.4427(7) Å, β = 97.370(4)°, U = 3710.8(4) Å^3, Z = 4, D_c = 1.488 Mg m^{-3}, μ(Mo Kα) = 0.714 mm^{-1}, T = 123 K. Total 27 891 reflections, 4262 unique, R_{int} = 0.100. Refinement of 2701 reflections (281 parameters) with $I > 2\sigma(I)$ converged at final R_1 = 0.0684 (R_1 all data = 0.1125), wR_2 = 0.0548 (wR_2 all data = 0.0814), gof = 1.0131.

[Cu(4)(NCMe)₂][PF₆]

$C_{18}H_{18}CuF_6N_4O_2P$, $M = 530.87$, orange needle, monoclinic, space group $P2_1/c$, $a = 13.2830(3)$, $b = 7.4327(2)$, $c = 21.8910(4)$ Å, $\beta = 105.697(1)°$, $U = 2080.66(8)$ Å³, $Z = 4$, $D_c = 1.695$ Mg m⁻³, μ(Mo Kα) = 1.204 mm⁻¹, $T = 123$ K. Total 46 113 reflections, 7963 unique, $R_{int} = 0.025$. Refinement of 6006 reflections (289 parameters) with $I > 2\sigma(I)$ converged at final $R_1 = 0.0242$ (R_1 all data = 0.0319), w$R_2 = 0.0249$ (wR_2 all data = 0.0372), gof = 1.0702.

[Ru(bpy)₂(1)][PF₆]₂·2.2MeCN

$C_{37.40}H_{32.60}F_{12}N_{8.20}O_2P_2Ru$, $M = 1019.94$, red block, monoclinic, space group $P2_1/n$, $a = 14.0032(8)$, $b = 19.8547(13)$, $c = 15.4352(10)$ Å, $\beta = 100.742(3)°$, $U = 4216.2(5)$ Å³, $Z = 4$, $D_c = 1.607$ Mg m⁻³, μ(Mo Kα) = 0.546 mm⁻¹, $T = 123$ K. Total 81 523 reflections, 10 482 unique, $R_{int} = 0.054$. Refinement of 7564 reflections (586 parameters) with $I > 2\sigma(I)$ converged at final $R_1 = 0.0409$ (R_1 all data = 0.0580), w$R_2 = 0.0415$ (wR_2 all data = 0.0593), gof = 1.0280.

[Ru(bpy)₂(2)][PF₆]₂·0.5H₂O

$C_{33}H_{27}F_{12}N_6O_{2.50}P_2Ru$, $M = 9937.60$, red block, monoclinic, space group $P2_1/c$, $a = 16.8253(9)$, $b = 9.7782(6)$, $c = 24.9831(15)$ Å, $\beta = 93.754(3)°$, $U = 4101.4(4)$ Å³, $Z = 4$, $D_c = 1.518$ Mg m⁻³, μ(Mo Kα) = 0.553 mm⁻¹, $T = 123$ K. Total 53 770 reflections, 10 249 unique, $R_{int} = 0.178$. Refinement of 5473 reflections (514 parameters) with $I > 2\sigma(I)$ converged at final $R_1 = 0.1106$ (R_1 all data = 0.1854), w$R_2 = 0.0870$ (wR_2 all data = 0.1203), gof = 1.0306.

Results and discussion

Ligand synthesis and characterization

Ligands **1** and **2** were prepared as previously reported.[20,21] Compounds **3** and **4** were synthesized by condensation of 6-methylpyridine-2-carbaldehyde with 4-amino- or 3-aminobenzoic acid, respectively. The electrospray mass spectra of methanol solutions of **1**, **2**, **3** and **4** exhibited peaks corresponding to [M + H]⁺ and [M + Na]⁺, as well as a peak at m/z 281.2 (for **1**, **2**) or 295.1 (for **3**, **4**) corresponding to [M + MeOH + Na]⁺. The previous reports of **1** and **2** did not include detailed NMR spectroscopic data. Our attempts to obtain clean ¹H NMR spectra for any of the four ligands in CD₃OD solution were hampered by the equilibria shown in eqn (1).
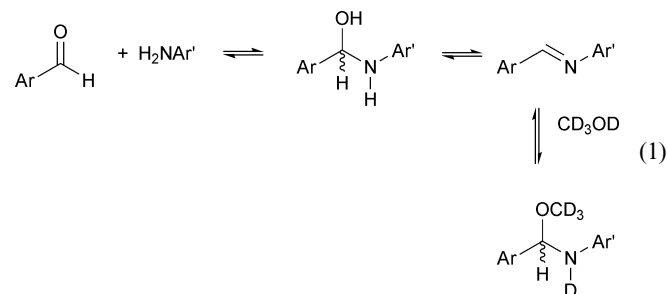
For each ligand, the presence of the imine was confirmed by the appearance of a singlet close to δ 8.6 ppm, while either or both of the saturated amino derivatives shown in eqn (1) gave rise to a diagnostic singlet at $\approx \delta$ 5.7 ppm assigned to the C*H*(OCD₃) or C*H*(OH) proton. Each spectrum also exhibited two low intensity subspectra corresponding to the corresponding pyridine-2-carbaldehyde and aminobenzoic acid. Spectra were assigned by COSY, comparison of relative integrals starting from the signals at δ 8.6 and 5.7 ppm, and comparison with CD₃OD solutions of authentic samples of pyridine-2-carbaldehyde, 6-methylpyridine-2-carbaldehyde and 3- or 4-aminobenzoic acid. Fig. 1 illustrates the distribution of species in a CD₃OD solution of ligand **1**, and the situation is similar for ligands **2**, **3** and **4**. The ¹H NMR spectrum of a solution of **1** in DMSO-d_6 revealed that **1** rather than the saturated amino derivatives was the dominant solution species in this solvent, although significant speciation persisted.
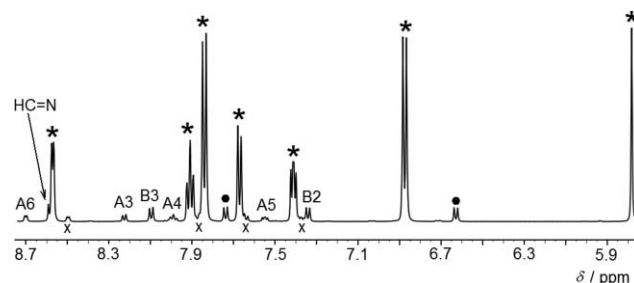

Fig. 1 500 MHz NMR spectrum of a CD₃OD solution of ligand **1** at room temperature. The assigned signals (see Scheme 1) correspond to **1**. Signals from a saturated amino derivative (eqn (1)) are labelled *, those from 4-aminobenzoic acid with ●, and those from pyridine-2-carbaldehyde with × (the aldehyde proton appears at δ 10.0 ppm and is not shown).

Ligands **1**, **2**, **3** and **4** appear to be significantly less stable in solution than the parent ligand **5** (Scheme 1). For **5**, it has been reported that an acetone-d_6 solution of the imine contains very minor peaks ($\approx$5%) corresponding to amine and aldehyde formed upon hydrolysis.[28] The presence of the carboxylic acid functionality could activate the imine towards nucleophilic attack by methanol (eqn (2)) leading to the observed solution speciation of ligands **1** to **4**. The presence of at least four species in each solution made it impossible to unambiguously interpret the ¹³C NMR spectra.

(2)
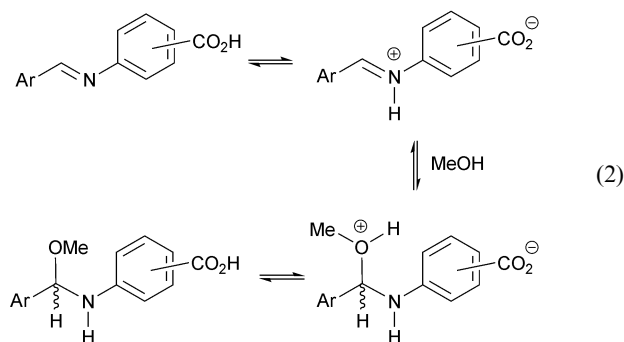
Despite the solution speciation, complexation of ligands **1**–**4** is expected to favour the imine form as illustrated in, for example, the work of Nitschke in which ligands are assembled *in situ* in the presence of copper(I).[17]

(1)

For each ligand, the presence of the imine was confirmed by the appearance of a singlet close to δ 8.6 ppm, while either

Ruthenium(II) complexes

Treatment of *cis*-[Ru(bpy)$_2$Cl$_2$] with **1** or **2** under microwave conditions resulted, after ion exchange, in the formation of [Ru(bpy)$_2$(**1**)][PF$_6$]$_2$ or [Ru(bpy)$_2$(**2**)][PF$_6$]$_2$ in moderate yields. In the electrospray mass spectrum of each complex, peak envelopes at *m/z* 785 and 320 exhibited the expected isotope patterns for [M − PF$_6$]$^+$ and [M − 2PF$_6$]$^{2+}$, respectively. Coordination of ligands **1** and **2** is immediately confirmed by the shift to lower frequency of the signal arising from pyridine H^{A6} (δ 8.70 to 7.83 ppm for **1**, and δ 8.68 to 7.83 ppm for **2**). Fig. 2 illustrates that each pyridine ring proton is unique. The spectra were assigned (Scheme 3) using COSY, NOESY, HMQC and HMBC techniques. Among the pyridine H^6 protons, H^{E6} is distinct from H^{A6}, H^{C6}, H^{D6} and H^{F6} because it lies over the imine group whereas each of the latter protons lies over the π-cloud of an adjacent pyridine ring. This causes the signals for H^{A6}, H^{C6}, H^{D6} and H^{F6} to be shifted to lower frequency upon coordination to the metal ion while H^{E6} is little perturbed. The assignments shown in Fig. 2(a) for [Ru(bpy)$_2$(**1**)]$^{2+}$ are consistent with those reported for [Ru(bpy)$_2$(**5**)]$^{2+}$ (see Scheme 1 for ligand **5**).[28] However, it is noteworthy that the signal for proton H^{D3}, and to a lesser extent that for H^{D4}, appears at lower frequency than the analogous proton in [Ru(bpy)$_2$(**5**)]$^{2+}$ as a consequence of

their location over the carboxylic acid group in [Ru(bpy)$_2$(**1**)]$^{2+}$. The fact that the signals for protons H^{B2} and H^{B3} appear as sharp doublets indicates that the C$_6$H$_4$CO$_2$H substituent undergoes fast rotation about the N–C$_{arene}$ bond on the NMR timescale at room temperature. On going from [Ru(bpy)$_2$(**1**)]$^{2+}$ to [Ru(bpy)$_2$(**2**)]$^{2+}$, the symmetry of the imino ligand is lowered, and all the protons in ring B become inequivalent. A comparison of Fig. 2(a) and 2(b) illustrates that the pyridine protons are unaffected by the change in the position of the carboxylic functionality.

The electronic absorption spectra of MeCN solutions of [Ru(bpy)$_2$(**1**)][PF$_6$]$_2$ and [Ru(bpy)$_2$(**2**)][PF$_6$]$_2$ are almost superimposable (Fig. 3). Each is dominated by an intense ligand-based band at 287 nm. The red colour of the complexes originates from broad, overlapping MLCT absorptions centred at 431 and 482 nm in [Ru(bpy)$_2$(**1**)][PF$_6$]$_2$, and 435 and 482 nm in [Ru(bpy)$_2$(**2**)][PF$_6$]$_2$. The flattened, double-humped shape of the band in the visible region mimics that reported for [Ru(bpy)$_2$(**5**)]$^{2+}$.[28] Irradiation of [Ru(bpy)$_2$(**1**)][PF$_6$]$_2$ at 455 nm gives rise to an emission at 607 nm with two lower energy shoulders (642 and 781 nm). Changing λ_{ex} to 430 or 480 nm results in a decrease in the intensity of the emission at 607 nm. Analogous emission behaviour was observed for [Ru(bpy)$_2$(**2**)][PF$_6$]$_2$ with λ_{em} = 606 nm and shoulders at 680 and 775 nm.

Fig. 3 Electronic absorption spectra of MeCN solutions of [Ru(bpy)$_2$(**1**)][PF$_6$]$_2$ ($\cdots$) and [Ru(bpy)$_2$(**2**)][PF$_6$]$_2$ (---).
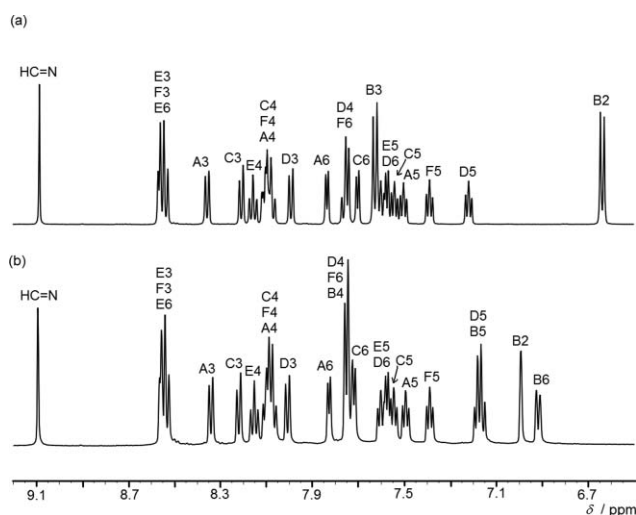
Fig. 2 500 MHz ^{1}H NMR spectra (CD$_3$CN, room temperature) of (a) [Ru(bpy)$_2$(**1**)][PF$_6$]$_2$ and (b) [Ru(bpy)$_2$(**2**)][PF$_6$]$_2$ (region δ 9.2 to 6.5 ppm). See Scheme 3 for labelling scheme.
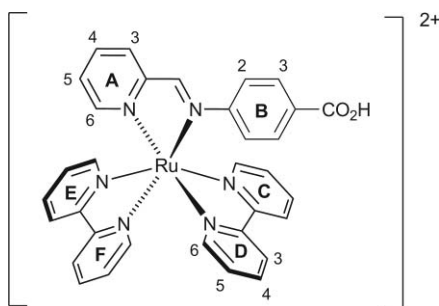
Scheme 3 Ring labelling for NMR spectroscopic assignments in [Ru(bpy)$_2$(**1**)]$^{2+}$. An analogous scheme is used in [Ru(bpy)$_2$(**2**)]$^{2+}$.
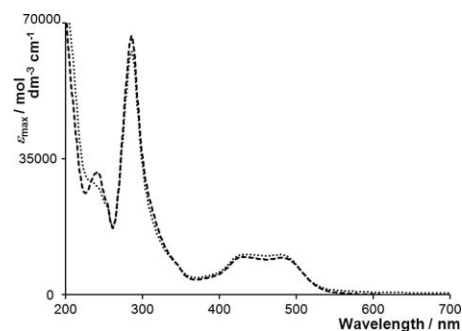
Crystals of [Ru(bpy)$_2$(**1**)][PF$_6$]$_2$·2.2MeCN suitable for X-ray diffraction were grown by slow diffusion of Et$_2$O into an MeCN solution of the complex. Fig. 4 presents the structure of the [Ru(bpy)$_2$(**1**)]$^{2+}$ cation and pertinent bond parameters are listed in the caption. The structure determination confirms the presence of three chelating ligands around an octahedrally coordinated ruthenium(II) centre. Bond parameters are unexceptional. Of relevance to the NMR spectroscopic discussion above is the fact that the C40–H401 bond points towards imine atom N2, although the N2$\cdots$H401 contact is long (2.77 Å). Pairs of molecules are associated through a hydrogen-bonded, centrosymmetric carboxylic acid dimer motif (O1H1$\cdots$O2^i = 1.81, O1$\cdots$O2^i = 2.628(3) Å, O1–H1$\cdots$O2^i = 176°, symmetry code i = 1 − x, 1 − y, 1 − z). The {CO$_2$H$\cdots$HO$_2$C} unit is sandwiched between two bpy domains of adjacent cations (Fig. 5(a)) with the distance between the plane of the {CO$_2$H$\cdots$HO$_2$C} unit to that of each bpy unit being 3.44 Å. These interactions involve the bpy ligands containing atoms N5^{ii}/N6^{ii} and N5^{iii}/N6^{iii} (symmetry codes ii = 3/2 − x, 1/2 + y, 3/2 − z; iii = −1/2 + x, 1/2 − y, −1/2 + z) and also extends to the pyridine ring to which the CO$_2$H functionality is attached. The remaining bpy ligands (those containing atoms
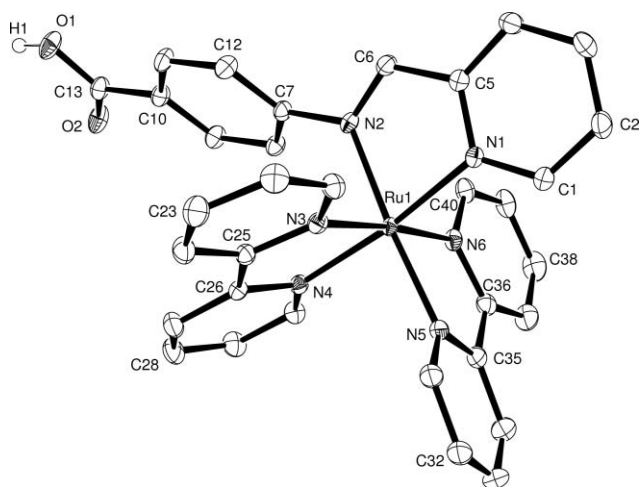
Fig. 4 Structure of the $[Ru(bpy)_2(1)]^{2+}$ cation in $[Ru(bpy)_2(1)][PF_6]_2 \cdot 2.2MeCN$ (ellipsoids plotted at the 40% probability level); H atoms except for the CO_2H group omitted. Atom H401 (see text) is attached to C40. Important bond parameters: Ru1–N1 = 2.058(2), Ru1–N2 = 2.059(2), Ru1–N3 = 2.066(2), Ru1–N4 = 2.071(2), Ru1–N5 = 2.059(2), Ru1–N6 = 2.054(2), N2–C6 = 1.297(3), N2–C7 = 1.435(3), C5–C6 = 1.456(3), O1–C13 = 1.317(3), O2–C13 = 1.225(3), C10–C13 = 1.487(3) Å; N1–Ru1–N2 = 77.85(8), N3–Ru1–N4 = 78.46(8), N5–Ru1–N6 = 78.50(9), C6–N2–C7 = 119.2(2), C5–C6–N2 = 116.5(2), O1–C13–O2 = 123.9(2)°.

N3/N4 and N3^{iv}/N4^{iv}, symmetry code iv = 1 − x, −y, 1 − z) associate into π-stacked pairs at a separation of 3.39 Å. Overall, the different sets of face-to-face π-interactions lead to the assembly of sheets (Fig. 5(b)) which are stacked to give a layer structure. The $[PF_6]^-$ ions and MeCN molecules occupy the cavities between the sheets and engage in extensive F···H–C$_{aromatic}$ and N···H–C$_{aromatic}$ interactions. Significantly, crystals of $[Ru(bpy)_2(1)][PF_6]_2 \cdot 2.2MeCN$ readily cleave into sheets.

Crystals of $[Ru(bpy)_2(2)][PF_6]_2 \cdot 0.5H_2O$ were grown by slow diffusion of Et_2O into a MeCN solution of the complex. Although the crystal quality allowed the structure to be solved, the refined result presented in Fig. 6(a) shows anisotropic displacement parameters that suggest disorder or other problems. However, the structure determination was sufficient to confirm the expected coordination geometry of the metal atom and the chelating mode of ligand **2**. A water molecule (modelled with a half occupancy for atom O3, and the H atoms for which could not be located in the difference map) is closely associated with the $[Ru(bpy)_2(2)]^{2+}$ cation (O2···O3 = 2.732(14) Å). The carboxylic acid hydrogen atom is in a calculated position and gives a reasonable hydrogen bonded interaction (O2H2···O3 = 1.87 Å, O2–H2···O3 = 156°). The presence of the water molecules prevents the formation of carboxylic acid dimers as observed in $[Ru(bpy)_2(1)][PF_6]_2 \cdot 2.2MeCN$. Instead, the free carbonyl group C33O1 forms a non-classical hydrogen bond with a pyridine unit of an adjacent cation (O1···H71^{i}C7^i = 2.33, O1···C7^i = 3.219(13) Å, O1···H71^{i}C7^i = 160°; symmetry code i = 1 − x, 1/2 + y, 3/2 − z). The repetition of these interactions results in the formation of undulating ribbons of cations through the lattice (Fig. 6(b)). The ordered $[PF_6]^-$ ions occupy the cavities between the cations, interacting with them through efficient F···H–C$_{aromatic}$ contacts.

(a)

(b)
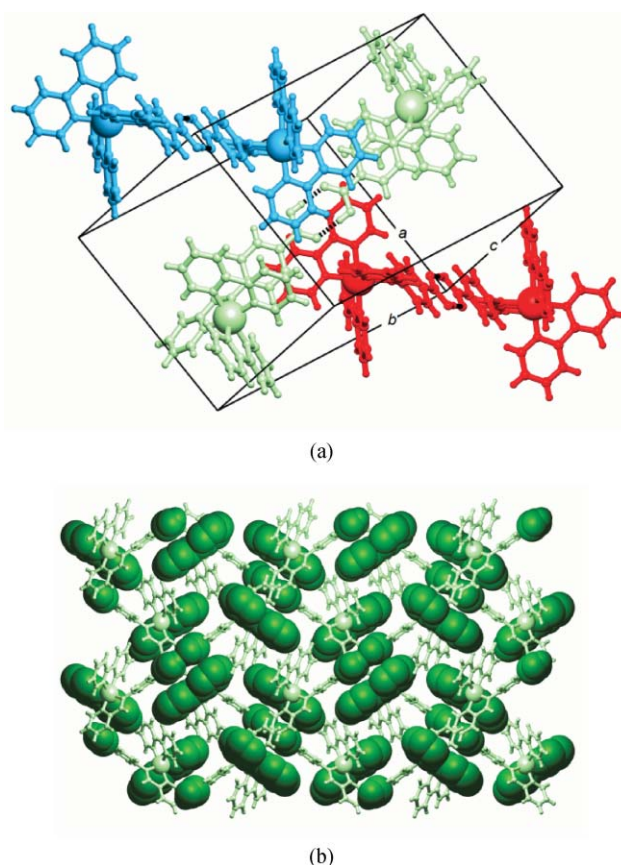
**Fig. 5** (a) π-Stacking of three cationic, hydrogen-bonded (black hashed lines) dimers in $[Ru(bpy)_2(1)][PF_6]_2 \cdot 2.2MeCN$. (b) A combination of bpy–{CO_2H…HO_2C}–bpy (dark green, space-filling) and bpy–bpy (pale green, ball-and-stick) face-to-face interactions lead to the assembly of sheets. The assembly is viewed down the a-axis.

Copper(I) complexes

The reaction of two equivalents of ligand **1** with $[Cu(NCMe)_4][PF_6]$ resulted in the formation of a copper(I) complex which proved to be poorly stable in solution. We therefore turned our attention to ligands **3** and **4** (Scheme 1) in which a methyl substituent is present in the 6-position of the pyridine ring. When $[Cu(NCMe)_4][PF_6]$ was treated with two equivalents of ligand **3** or **4**, red-brown $[Cu(3)_2][PF_6]$ or $[Cu(4)_2][PF_6]$ was obtained. The electrospray mass spectrum of each complex exhibited a peak envelope corresponding to [M − PF_6]$^+$ (m/z 543.0) with the correct isotope distribution. The ^1H NMR spectrum of a CD_3CN solution of each complex was consistent with one ligand environment. The singlet for the imino proton appeared at δ 9.08 ppm in $[Cu(3)_2]^+$ and δ 9.15 ppm in $[Cu(4)_2]^+$ compared to δ 8.56 and 8.57 ppm in free ligands **3** and **4**, respectively. The CD_3CN solution ^1H and ^{13}C NMR spectra of $[Cu(3)_2][PF_6]$ were assigned using COSY, HMQC and HMBC methods. At room temperature, the signals for H^{B2} and H^{B3} (Scheme 4) appear as somewhat broadened doublets with a reduced coupling constant of ≈6 Hz. This is consistent with the $C_6H_4CO_2H$ substituent undergoing hindered rotation about the N–C$_{arene}$ bond on the NMR timescale. The doublets for H^{A5} and H^{A3} were distinguished by the observation in the HMBC spectrum of a cross peak from the methyl proton signal (δ 2.43 ppm) to the
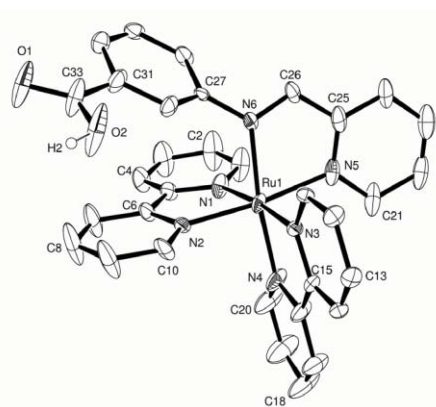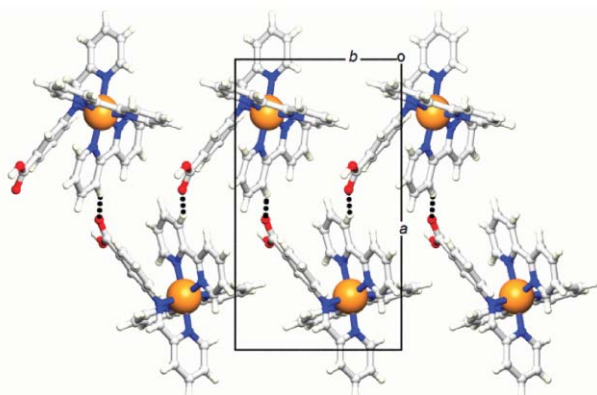
Fig. 6 (a) Structure of the $[Ru(bpy)_2(\mathbf{2})]^{2+}$ cation in $[Ru(bpy)_2(\mathbf{2})][PF_6]_2 \cdot 0.5H_2O$ (ellipsoids plotted at 30% probability level); H atoms except for the CO_2H group omitted. Selected bond distances and angles: Ru1–N1 = 2.078(6), Ru1–N2 = 2.054(6), Ru1–N3 = 2.056(5), Ru1–N4 = 2.023(7), Ru1–N5 = 2.094(6), Ru1–N6 = 2.051(6), N6–C26 = 1.306(9), N6–C27 = 1.405(9), C33–O1 = 1.251(10), C33–O2 = 1.313(13) Å; N1–Ru1–N2 = 78.9(2), N3–Ru1–N4 = 79.7(2), N5–Ru1–N6 = 76.7(2), C26–N6–C27 = 119.0(6), O1–C33–O2 = 120.3(11)°. (b) Part of one ribbon of cations assembled through non-classical hydrogen bonds (see text).

signal for carbon atom C^{A5} (δ 127.3 ppm). The decrease in ligand symmetry on going from $[Cu(\mathbf{3})_2]^+$ to $[Cu(\mathbf{4})_2]^+$ was confirmed by an increase in the number of signals in the ^{13}C NMR spectrum of a CD_3CN solution of $[Cu(\mathbf{4})_2][PF_6]$. However, the aromatic region of the ^1H NMR spectrum exhibited a considerable overlapping of signals. Confirmation of their assignments was aided by the ^1H NMR spectrum of $[Cu(\mathbf{4})(NCMe)_2]^+$, prepared as the hexafluoridophosphate salt by treatment of $[Cu(NCMe)_4][PF_6]$ with one equivalent of ligand **4**. The signals for the seven aromatic protons in $[Cu(\mathbf{4})(NCMe)_2][PF_6]$ were well separated. The four ring B proton signals were broadened as a consequence of the hindered rotation of $C_6H_4CO_2H$ substituent about the N–C_{arene} bond. Assignment of the four corresponding signals in the ^{13}C NMR spectrum from the HMQC spectrum revealed broad signals for C^{B2}, C^{B5} and C^{B6} and a sharp signal for C^{B4} (*i.e.* the carbon atom least affected by ring rotation). This distinction between the signals for C^{B4} and C^{B6} allowed proton signals H^{B4} and H^{B6} to be distinguished in the ^1H NMR spectrum. Fig. 7 illustrates the effect
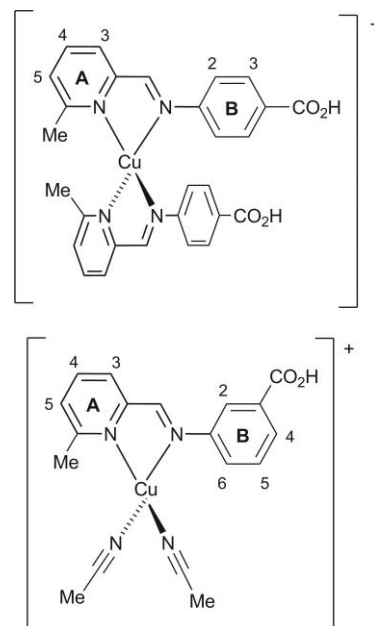
Scheme 4 Atom labelling for NMR spectroscopic assignments in $[Cu(\mathbf{3})_2]^+$ and $[Cu(\mathbf{4})(NCMe)_2]^+$. An analogous scheme is used in $[Cu(\mathbf{4})_2]^+$.
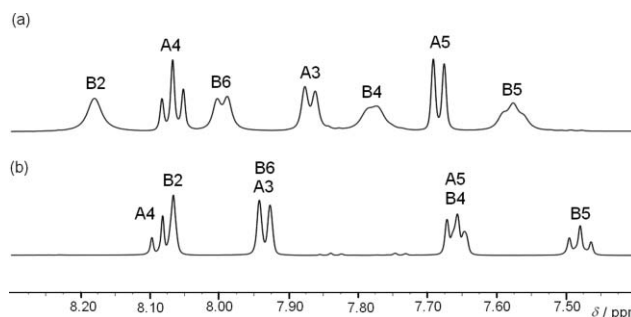

Fig. 7 500 MHz ^1H NMR spectra of a CD_3CN solution of (a) $[Cu(\mathbf{4})(NCMe)_2][PF_6]$ and (b) $[Cu(\mathbf{4})_2][PF_6]$ (region δ 8.3 to 7.4 ppm).

on the aromatic region of the ^1H NMR spectrum of substituting the two MeCN ligands in $[Cu(\mathbf{4})(NCMe)_2]^+$ by a second ligand **4**. A comparison of the peak shapes in Fig. 7(a) and 7(b) reveals that the arene ring rotates rapidly on the NMR timescale in $[Cu(\mathbf{4})_2]^+$ but is hindered in $[Cu(\mathbf{4})(NCMe)_2]^+$. The solid state structural data presented below are consistent with the methyl groups of the MeCN ligands hindering the dynamic process.

An acetonitrile solution of each of the copper(I) complexes exhibits a relatively weak MLCT band close to 500 nm. An intense absorption at ≈310 nm and a high energy tail into the vacuum-UV are assigned to ligand-based $\pi^* \leftarrow \pi$ transitions. The spectra of $[Cu(\mathbf{3})_2][PF_6]$ (Fig. 8) and $[Cu(\mathbf{4})_2][PF_6]$ also exhibit a ligand-based absorption at 260 and 282 nm, respectively.

Crystals of $[Cu(\mathbf{3})_2][PF_6] \cdot 2DMF$ were grown by slow diffusion of Et_2O into a DMF solution of the complex. and Fig. 9 depicts the structure of the cation in the complex. Atom Cu1 is located on the special position 0, y, 1/4, so that the two ligands in the $[Cu(\mathbf{3})_2]^+$ ion are related by a 2-fold axis. The coordination environment about the copper atom is distorted tetrahedral, with the angle between the planes of the chelate rings being 81.5°. The P atom in the $[PF_6]^-$ anion resides on the special position 0, y, 1/4, and the disordered
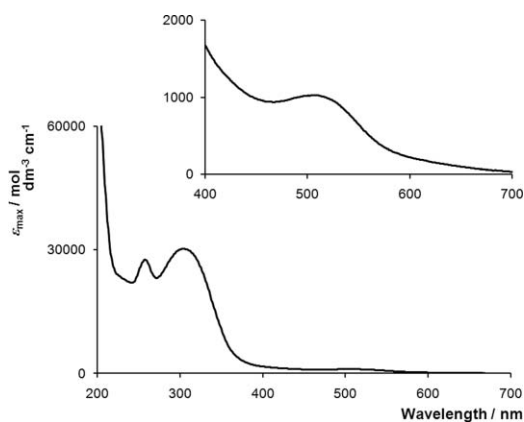
Fig. 8 Electronic absorption spectrum of a MeCN solution of [Cu(**3**)₂][PF₆]. The insert shows an expansion of the MLCT band.
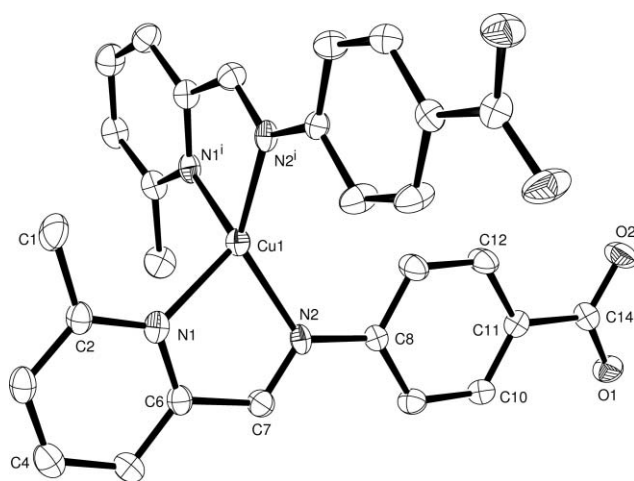

Fig. 9 Structure of the [Cu(**3**)₂]⁺ cation in [Cu(**3**)₂][PF₆]·2DMF (ellipsoids plotted at the 40% probability level); H atoms omitted for clarity. Symmetry code $i = -x$, y, $1/2 - z$. Important bond parameters: Cu1–N1 = 2.032(3), Cu1–N2 = 2.025(3), N2–C7 = 1.282(5), N2–C8 = 1.416(4), O1–C14 = 1.256(4), O2–C14 = 1.282(5) Å; N1–Cu1–N2 = 81.68(12), N1ⁱ–Cu1–N1 = 111.46(17), N1ⁱ–Cu1–N2 = 126.24(12), N2ⁱ–Cu1–N2 = 133.29(16), C7–N2–C8 = 122.2(3), O2–C14–O1 = 122.7(4)°.

anion has been modelled over atom positions related by a 2-fold axis. The presence of the DMF solvent molecules in the lattice prevents the formation of {CO₂H···HO₂C} dimeric motifs, and the dominant packing interactions are hydrogen bonding between cations and DMF molecules, and π-stacking between C₆H₄CO₂H arene rings (ring separation = 3.42 Å). The oxygen atom of the DMF molecule in the asymmetric unit is disordered and has been modelled over two equal occupancy sites (O3 and O4) which are, respectively, 2.507(6) and 2.442(7) Å away from atoms O2 and O1 of the CO₂H unit. The hydrogen atoms bonded to carboxylate oxygen atoms and the C=O carbon atom in DMF could not be located in the difference map, most probably because of each being disordered over two positions.

X-Ray quality crystals of [Cu(**4**)(NCMe)₂][PF₆] were grown by slow diffusion of Et₂O into an MeCN solution of the compound. The structure is ordered and the carboxylic acid H atom was located from the difference map. Fig. 10 shows the structure of the [Cu(**4**)(NCMe)₂]⁺ cation and the caption gives selected
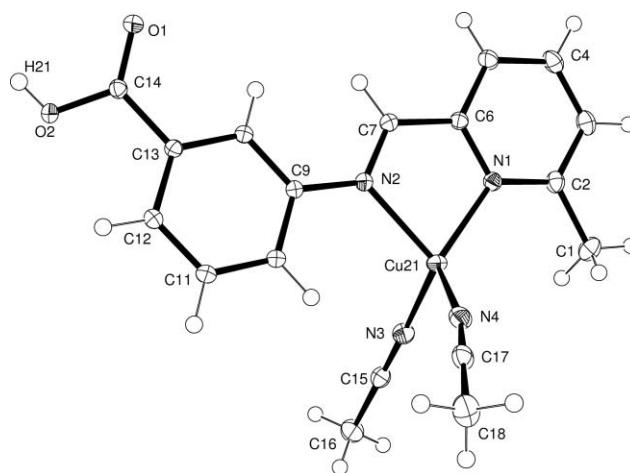

Fig. 10 Structure of the [Cu(**4**)(NCMe)₂]⁺ cation in [Cu(**4**)(NCMe)₂][PF₆] (ellipsoids plotted at the 50% probability level). Important bond parameters: Cu21–N1 = 2.0342(8), Cu21–N2 = 2.1100(8), Cu21–N3 = 1.9568(9), Cu21–N4 = 1.9708(9), N2–C7 = 1.2836(11), N2–C9 = 1.4198(12), O1–C14 = 1.2209(11), O2–C14 = 1.3204(11), N3–C15 = 1.1427(13), N4–C17 = 1.1413(13) Å; N1–Cu21–N2 = 80.42(3), N1–Cu21–N3 = 123.18(3), N2–Cu21–N3 = 114.64(3), N1–Cu21–N4 = 122.75(3), N2–Cu21–N4 = 110.92(3), N3–Cu21–N4 = 103.11(4), C7–N2–C9 = 122.33(8), Cu21–N3–C15 = 169.45(8), Cu21–N4–C17 = 167.99(9)°.

bond distances and angles. The angle between the least squares planes of the chelate ring and the N3Cu21N4 unit is 88.19(5)°, consistent with a near tetrahedral environment for the copper atom. However, the CuNCC (coordinated MeCN) units are significantly bowed (Cu21–N3–C15 = 169.45(8), Cu21–N4–C17 = 167.99(9)°). This distortion appears to be caused by tight cation–anion pairing in the crystal lattice. Each [PF₆]⁻ ion is held within the two arms of the Cu(NCMe)₂ unit (F2···C15 = 3.1353(12), F2···C17 = 3.1684(13), F3···C15 = 3.2412(13), F4···H183 = 2.74, F4···C18 = 3.1152(14), F4···C17 = 3.0636(13) Å) and also has close contacts to the phenyl ring (F4···H101 = 2.58, F4···H111 = 2.69 Å). The ion pairs assemble into chains (Fig. 11) by virtue of hydrogen bonding between adjacent CO₂H
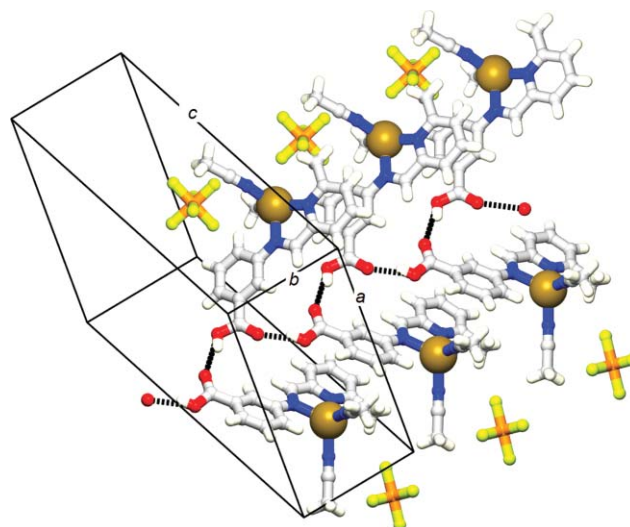
**Fig. 11** Formation of hydrogen-bonded chains of cations, and close cation–anion pairing in [Cu(**4**)(NCMe)₂][PF₆].

Table 1 Current–voltage characteristic data for DSCs. Cells were constructed as detailed in the experimental section, and the anion was [PF$_6$]$^-$ for all the cationic dyes

| Dye	J_{sc}/mA cm^{-2}	V_{oc}/mV	FF	η_{global}/%	λ_{max}/nm soln^a	λ_{max}, TiO$_2$/nm (Abs/a.u.)	Coverage/nmol cm^{-2}
[Ru(bpy)$_2$(**1**)]$^{2+}$	0.19	302	0.41	0.02	431, 486	442, 481 (0.71)	74
[Ru(bpy)$_2$(**2**)]$^{2+}$	0.17	315	0.43	0.02	435, 482	434, 480 (0.35)	34
[Cu(**3**)$_2$]$^+$	0.84	442	0.61	0.23	511	512 (0.40)	400
[Cu(**4**)$_2$]$^+$	0.33	357	0.53	0.006	499	506 (0.45)	270
[Cu(**4**)(NCMe)$_2$]$^+$	0.40	387	0.52	0.008	502	506 (0.47)	185
N719	16	759	0.38	4.60	530	534 (1.04)	76

^{a} Values of ε_{max} for complexes reported in this paper are given in the experimental section.

groups (O2H21$\cdots$O1^i = 1.88, O2$\cdots$O1^i = 2.6463(10) Å, O2–H21$\cdots$O1^i = 160°); symmetry code $i = 1 - x$, $1/2 + y$, $1/2 - z$). Fig. 11 also illustrates that the chains are additionally supported by π-stacked pairs of pyridine and phenyl rings (distance between the rings containing atoms N1 and C13^{ii} = 3.42 Å, symmetry code ii: x, $1 - y$, z). Although the accommodation of the [PF$_6$]$^-$ anion within the pocket between the Cu(NCMe)$_2$ unit and the phenyl ring is confirmed for the solid state, it is of interest to note that such an interaction would also explain why hindered rotation of the C$_6$H$_4$CO$_2$H unit about the N–C$_{arene}$ bond is observed in solution.

Performance of DSCs

The incorporation of a carboxylic acid functionality in each of ligands **1** to **4** was expected to facilitate binding of the ruthenium(II) or copper(I) complexes to TiO$_2$ (Scheme 2), and in the cases of [Cu(**3**)$_2$]$^+$ and [Cu(**4**)$_2$]$^+$, the geometry of the complexes should orient both carboxylate groups onto the TiO$_2$ surface (Scheme 2). Fabrication of DSCs using the new dyes and the determination of the device characteristics are described in the experimental section. A comparison of the performances of these DSCs is presented in Table 1, with the ruthenium dye N719 (measured under the same conditions as the new dyes) being used as an internal standard. In MeCN solution, each ruthenium(II) complex exhibits a broad MLCT band (Fig. 3), and a similarly shaped absorption with approximately equal intensity components is observed for each ruthenium(II) dye adsorbed onto TiO$_2$ (Table 1). Although the surface coverage of [Ru(bpy)$_2$(**1**)][PF$_6$]$_2$ and [Ru(bpy)$_2$(**2**)][PF$_6$]$_2$ appears to be comparable with that of the standard dye N719, the current and global efficiencies are low. In part, this is because each of [Ru(bpy)$_2$(**1**)]$^{2+}$ and [Ru(bpy)$_2$(**2**)]$^{2+}$ only contains one carboxylate anchoring group. Both [Cu(**4**)$_2$][PF$_6$] and [Cu(**4**)(NCMe)$_2$][PF$_6$] show relatively high surface coverage on TiO$_2$ (Table 1), but the performance characteristics are disappointing. Significantly, the change from two anchoring groups to one on going from [Cu(**4**)$_2$]$^+$ to [Cu(**4**)(NCMe)$_2$]$^+$ does not lead to a corresponding decrease in global efficiency or current per nanomole of surface-bound dye. Although the surface coverage of [Cu(**3**)$_2$][PF$_6$] (the absorption spectrum of which is shown in Fig. 12) is promising, the short circuit current density (J_{sc}) is not correspondingly high and the overall performance judged from the value of J_{sc} in mA per nanomole of surface-bound [Cu(**3**)$_2$]$^+$ is analogous to that of [Cu(**4**)$_2$][PF$_6$].

The complexes incorporating carboxylic acid functionalized N-phenylpyridin-2-ylmethanimine ligands proved to be less
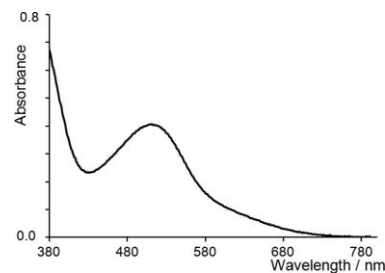
Fig. 12 Electronic spectrum of [Cu(**3**)$_2$][PF$_6$] adsorbed onto TiO$_2$ from a DMF solution (see experimental section). Compare with the insert in Fig. 8.

promising than the series of copper(I) complexes of 6,6′-disubstituted 2,2′-bipyridine dicarboxylic acids that we have reported earlier.[7,12] Although the performance of the new DSCs is disappointing, it may be rationalized. For efficient injection into the TiO$_2$ semiconductor it is necessary to have (i) good binding to the surface, (ii) good coverage, and (iii) good electronic matching of the surface with the ligands. In our complexes requirement (ii) is fulfilled and (i) is not too weak. However, the most effective injection occurs when the LUMO of the complex lies on the passway to the semiconductor. Calculations at the DFT B3LYP level on these complexes indicate that the character of the LUMO (which equates to the MLCT transient species) is more than 90% on the pyridine rings.

Conclusions

Ligands **1**–**4** have been designed to allow copper(I) complexes [CuL$_2$]$^+$ to bind to a TiO$_2$ surface through the simultaneous use of two carboxylate anchoring domains. Complexes [Ru(bpy)$_2$(**1**)][PF$_6$]$_2$, [Ru(bpy)$_2$(**2**)][PF$_6$]$_2$, [Cu(**3**)$_2$][PF$_6$], [Cu(**4**)$_2$][PF$_6$] and [Cu(**4**)(NCMe)$_2$][PF$_6$] have been synthesized and fully characterized. DSCs fabricated using the ruthenium(II) complexes perform poorly. The copper(I) complexes show good or very good surface coverage, and tuning of the electronic properties of the ligands and variation of the electrolyte are now required to enhance the efficiencies of the DSCs.

Acknowledgements

References

1 M. K. Nazeeruddin and M. Grätzel, *Struct. Bonding*, 2007, **123**, 113.

2 M. Grätzel, *Inorg. Chem.*, 2005, **44**, 6841.

3 A. S. Polo, M. K. Itokazu and N. Y. M. Iha, *Coord. Chem. Rev.*, 2004, **248**, 1343.

4 S. Ardo and G. J. Meyer, *Chem. Soc. Rev.*, 2009, **38**, 115.

5 S. Anderson, E. C. Constable, M. P. Dare-Edwards, J. B. Goodenough, A. Hamnett, K. R. Seddon and R. D. Wright, *Nature*, 1979, **280**, 571.

6 B. O'Regan and M. Grätzel, *Nature*, 1991, **353**, 737.

7 T. Bessho, E. C. Constable, M. Grätzel, A. Hernandez Redondo, C. E. Housecroft, W. Kylberg, Md. K. Nazeeruddin, M. Neuburger and S. Schaffner, *Chem. Commun.*, 2008, 3717.

8 N. Alonso-Vante, V. Ern, P. Chartier, C. O. Dietrich-Buchecker, D. R. McMillin, P. A. Marnot and J.-P. Sauvage, *Nouv. J. Chim.*, 1983, **7**, 3.

9 N. Alonso-Vante, J.-F. Nierengarten and J.-P. Sauvage, *J. Chem. Soc., Dalton Trans.*, 1994, 1649.

10 S. Sakati, T. Kuroki and T. Hamada, *J. Chem. Soc., Dalton Trans.*, 2002, 840.

11 A. Hernandez Redondo, E. C. Constable and C. E. Housecroft, *Chimia*, 2009, **63**, 205.

12 E. C. Constable, A. Hernandez Redondo, C. E. Housecroft, M. Neuburger and S. Schaffner, *Dalton Trans.*, 2009, 6634.

13 E. C. Constable, C. E. Housecroft, M. Neuburger, J. Price, A. Wolf and J. A. Zampese, *Inorg. Chem. Commun.*, 2010, **13**, 74.

14 W. W. Brandt, F. P. Dwyer and E. D. Gyarfas, *Chem. Rev.*, 1954, **54**, 959.

15 See for example: S.-L. Ma, X.-X. Sun, S. Gao, C.-M. Qi, H.-B. Huang and W.-X. Zhu, *Eur. J. Inorg. Chem.*, 2007, 846; S. Dehghanpor, N. Bouslimani, R. Weber and F. Mojahed, *Polyhedron*, 2007, **26**, 154; D. Schultz, Frédéric Biaso, A. R. M. Shahi, M. Geoffroy, K. Rissanen, L. Gagliardi, C. J. Cramer and J. R. Nitschke, *Chem.–Eur. J.*, 2008, **14**, 7180; M. Boiocchi, B. Colasson, L. Fabbrizzi and E. Monti, *Inorg. Chim. Acta*, 2007, **360**, 1163; J. R. Price, Y. Lan and S. Brooker, *Dalton Trans.*, 2007, 1807.

16 See for example: G. A. Ardizzoia, S. Brenna, F. Castelli and S. Galli, *Inorg. Chim. Acta*, 2009, **362**, 3507; B.-Y. Su and J.-S. Zhao, *Polyhedron*, 2006, **25**, 3289; J. Chen, Y. Huang, Z. Li, Z. Zhang, C. Wei, T. Lan and W. Zhang, *J. Mol. Catal. A: Chem.*, 2006, **259**, 133.

17 J. R. Nitschke, *Angew. Chem., Int. Ed.*, 2004, **43**, 3073; D. Schultz and J. R. Nitschke, *Proc. Natl. Acad. Sci. U. S. A.*, 2005, **102**, 11191; D. Schultz and J. R. Nitschke, *J. Am. Chem. Soc.*, 2006, **128**, 9887; V. E. Campbell, X. de Hatten, N. Delsuc, B. Kauffmann, I. Huc and J. R. Nitschke, *Chem.–Eur. J.*, 2009, **15**, 6138; J. Fan, J. W. Bats and M. Schmittel, *Inorg. Chem.*, 2009, **48**, 6338; R. J. Sarma, S. Otto and J. R. Nitschke, *Chem.–Eur. J.*, 2007, **13**, 9542.

18 G. Sprintschnik, H. W. Sprintschnik, P. P. Kirsch and D. G. Whitten, *J. Am. Chem. Soc.*, 1977, **99**, 4947.

19 G. J. Kubas, *Inorg. Synth.*, 1990, **28**, 68.

20 C.-F. Jiang, F.-P. Liang, Y. Li, X.-J. Wang, Z.-L. Chen and H.-D. Bian, *J. Mol. Struct.*, 2007, **842**, 109.

21 A. Menteş and M. E. Hanhan, *Transition Met. Chem.*, 2008, **33**, 91.

22 COLLECT Software, Nonius BV 1997-2001.

23 A. Altomare, G. Cascarano, G. Giacovazzo, A. Guagliardi, M. C. Burla, G. Polidori and M. Camalli, *J. Appl. Crystallogr.*, 1994, **27**, 435.

24 Z. Otwinowski and W. Minor, *Methods in Enzymology*, vol. 276, ed. by C.W. Carter, Jr and R.M. Sweet, 1997, Academic Press, New York, p. 307.

25 P. W. Betteridge, J. R. Carruthers, R. I. Cooper, K. Prout and D. J. Watkin, *J. Appl. Crystallogr.*, 2003, **36**, 1487.

26 L. J. Farrugia, *J. Appl. Crystallogr.*, 1997, **30**, 565.

27 I. J. Bruno, J. C. Cole, P. R. Edgington, M. K. Kessler, C. F. Macrae, P. McCabe, J. Pearson and R. Taylor, *Acta Crystallogr., Sect. B: Struct. Sci.*, 2002, **58**, 389.

28 A. C. G. Hotze, J. A. Faiz, N. Mourtzis, G. I. Pascu, P. R. A. Weber, G. J. Clarkson, K. Yannakopoulou, Z. Pikramenou and M. J. Hannon, *Dalton Trans.*, 2006, 3025.